






Trend analysis of precipitation extremes in Brazil: the role of atmospheric temperature

Análise da tendência de extremos de precipitação no Brasil: o papel da temperatura atmosférica

José Micael Ferreira da Costa¹ , Cleiton da Silva Silveira¹ , Alexandre Cunha Costa² ,
Antonio Duarte Marcos Junior¹ , Suellen Teixeira Nobre Gonçalves¹ 

ABSTRACT

There is evidence that the climate on the planet has been undergoing variations over the years, resulting in climate events that are becoming increasingly extreme, such as heavy raining. The objective of this study was to verify the behavior and tendency of heavy rain in Brazil, and possible correlations with atmospheric temperature. The methodology utilizes Climate Extremes Indices (CEI), and the Mann-Kendall Test (MKT) and Sen's Slope (SS) were applied in each of them to evaluate the statistical significance of the trends in climate extremes, as well as to measure the magnitudes, respectively. Then, Pearson's Correlate Coefficient (PCC) between indexes was calculated. The total period of analysis was between 1991 to 2022. The MKT and SS results presented tendencies of extreme rain increase in the South, North, parts of the Northeast and Southeast coastline, and the decrease trend in the Midwest, Southeast and North. There are, too, increase trends in the maximum (TX) and minimum temperature (TN) in the whole country. PCCs were significant, between total/extreme rainfall and temperature, as follows: Northeast and Southeast (negative PCCs for TX); North and South (positive PCCs for TN). There are some areas where the SS and PCCs presented non-linear interdependence between these climatic variables. Therefore, the changes in the climate pattern can contribute to the increase trend in extreme precipitation events in different areas of Brazil.

Keywords: heavy rainfall; trends; correlations; climate change.

RESUMO

Existem evidências de que o clima no planeta vem sofrendo variações ao longo dos anos, as quais têm gerado eventos climáticos que estão se tornando cada vez mais extremos, como os de chuvas intensas. O objetivo deste estudo foi verificar o comportamento e a tendência das chuvas extremas no Brasil e suas possíveis correlações com as tendências da temperatura atmosférica. A metodologia utilizou Índices de Extremos Climáticos e, em cada um deles, foi aplicado o Teste de Mann-Kendall (TMK) e a Declividade de Sen (DS) para avaliar a significância estatística das tendências dos extremos climáticos, assim como mensurar as magnitudes, respectivamente. Em seguida, foi calculado o coeficiente de correlação de Pearson (CCP) entre índices. O período total de análise foi de 1991 a 2022. Os resultados da TMK e DS mostraram tendência de aumento das chuvas extremas nas Regiões Sul, Norte, partes do Nordeste e na faixa litorânea do Sudeste e tendência de diminuição nas Regiões Centro-Oeste, Sudeste e Norte. Também houve tendência de aumento da temperatura máxima (TX) e mínima (TN) na maior parte do país. Os CCP foram significativos, entre as chuvas totais/extremas e as temperaturas, do seguinte modo: regiões Nordeste e Sudeste (CCP negativas para TX); Sul e Norte (CCP positivas para TN). Houve então locais onde as DS e os CCP apresentaram interdependência não linear entre essas variáveis climáticas. Assim, a mudança no padrão climático das temperaturas pode estar contribuindo para a tendência de aumento dos eventos extremos de precipitação em várias regiões do Brasil.

Palavras-chave: chuvas intensas; tendências; correlações; mudanças climáticas.

¹Universidade Federal do Ceará – Fortaleza (CE), Brazil.

²Universidade da Integração Internacional da Lusofonia Afro-Brasileira – Redenção (CE), Brazil.

Corresponding author: José Micael Ferreira da Costa – Departamento de Engenharia Hidráulica e Ambiental (DEHA) – Rua 5, 100 – Pres. Kennedy – CEP: 60355-636 – Fortaleza (CE), Brasil. E-mail: jmichaelcosta@gmail.com

Funding: Fundação Cearense de Apoio Ao Desenvolvimento Científico e Tecnológico (FUNCAP), Projeto: “Utilização da Previsão SUBSAZONAL na gestão de recursos hídricos e no risco climático da produtividade agrícola”, process number: PS1-0186-00326.01.00/21; and Conselho Nacional de Desenvolvimento Científico e Tecnológico (CNPq), process number: 306380/2023-4.

Conflicts of interest: the authors declare no conflicts of interest.

Received on: 05/15/2024. Accepted on: 03/17/2025.

<https://doi.org/10.5327/Z2176-94782123>



This is an open access article distributed under the terms of the Creative Commons license.

Introduction

The spatial and temporal variability of precipitation forms the basis for different research areas, such as territorial planning, agriculture, water resources, energy, natural disasters, and public health (Chagas et al., 2022; Costa et al., 2022; Freire et al., 2023). Due to global warming, an increase in the frequency, distribution, and intensity of extreme precipitation events can be observed. These events are characterized by intense rainfall, significantly above the region's historical average, and can be classified as high (above the 95th percentile) and extreme (above the 99th percentile) according to their frequency distribution. Such events trigger flooding, water accumulation, and wet mass movements. This intensification poses risks to public safety, infrastructural damage, disruption of water and energy supply, health hazards, economic impacts, devastation of agricultural and forested areas, and exacerbation of social disparities (Teixeira and Satyamurty, 2007; Grimm and Zilli, 2009; Lima et al., 2010; Marengo et al., 2016; Cardoso et al., 2020; Moreira et al., 2020; Rocha, 2021).

Nobre (2001) had already pointed out that rising air temperatures could accelerate the hydrological cycle, generating more water vapor in the atmosphere and leading to a higher frequency of extreme events such as hurricanes, droughts, and extreme rainfall. The relationship between temperature and precipitation has a physical basis: according to the Clausius-Clapeyron equation (Brown, 1951), the vapor pressure (VP) of water varies exponentially with temperature changes. At higher temperatures, more water vapor is required to reach saturation. This process occurs when an air parcel rises in the atmosphere, expands, and cools pseudo-adiabatically, increasing relative humidity (RH) due to the reduction of the saturation vapor pressure (SVP) of water (Lamb and Verlinde, 2011). When RH reaches 100%, the parcel becomes saturated, and condensation occurs, transitioning water from vapor to liquid form, leading to cloud droplet formation.

Therefore, the higher the temperature, the higher the SVP and the evaporation rate in the atmosphere, increasing the vapor disposition in the air. This relationship directly impacts the intensity, duration, and frequency of precipitation events. With more steam in the atmosphere and a higher SVP, the air can retain larger amounts of water vapor, slowing the condensation process, and reducing the frequency of rainfall. And although the frequency decreases, with higher accumulation of steam inside the clouds, there will also be a higher volume of water available to precipitate when this steam condenses, increasing the intensity and duration of the events. Therefore, the increase in temperatures around the planet can trigger the increase in extreme rainfall in different locations around the world (Pall et al., 2007).

Globally, the magnitude of extreme precipitation has increased (Donat et al., 2016). Maximum daily annual rainfall has grown by an average of 5.9 to 7.7%, which corresponds to the theoretical Clausius-Clapeyron increase (6-7%/°C) in the moisture holding capacity of the atmosphere due to higher temperatures (Fowler et al., 2021;

Sun et al., 2021). Extreme rains from October to December 2019 over East Africa formed one of the wettest seasons on record, leading to flooding and landslides, with initial estimates suggesting that more than 2.8 million people were negatively affected (Wainwright et al., 2021). In July 2021, extreme rainfall across Western Europe caused severe flooding and substantial impacts, where 200 thousand properties lost electricity, including more than 200 deaths and extensive infrastructure damage in Germany and the Benelux countries (Tradowsky et al., 2023). In the same month and year, there was torrential rain in Asia with a maximum intensity of 201.9 millimeters in a single hour and that led to major floods in Henan province, China, forcing more than one million people to move (Liang, 2022). In the United States, the 2017 Oroville Dam Crisis in California, which caused the evacuation of more than 180 thousand people, occurred due to heavy precipitation that led to extensive flooding in the region (Vahedifard et al., 2017; Hollins et al., 2018).

In Brazil, the National Water and Sanitation Agency (ANA) reports that in 2017, approximately three million people were impacted by floods and inundations (ANA, 2018). Each region of the country faces specific challenges regarding its ability to deal with the impacts of extreme events. This happens due to geographical, socioeconomic, and environmental differences, which influence the deficiencies of each location in the preparation and response to these events, as pointed out by the study of Perez et al. (2020). The South part of Brazil is historically the most affected by extreme precipitation events, facing significant risks due to its geography and lack of adequate infrastructure, which causes landslides and major floods (Palenzuela et al., 2019; Cardoso et al., 2020; Goudard and Mendonça, 2020; Teixeira and Prieto, 2020; Zandonadi, 2020). The Midwest, an area of large agricultural production, faces the threat of economic losses due to floods and storms (Silva and da Franca, 2021).

The Southeast, with its large metropolitan areas, has vulnerabilities in infrastructure and water supply. Additionally, hillside areas are more prone to landslides as extreme events increase (Caetano and Barbosa, 2019; Marengo et al., 2020; Tavares and Ferreira, 2020; Bonfim et al., 2020; Sanches, 2022). The Northeast, despite recurring drought episodes, has increasingly faced extreme precipitation and temperature events, where inadequate drainage infrastructure and shallow, poorly drainable soils exacerbate their impacts, particularly in urban and coastal areas (Alves et al., 2017; Sena et al., 2019; da Silva et al., 2020; Guedes and Silva, 2020; Duarte et al., 2021; Gonçalves et al., 2023). In the Northern region, deforestation combined with climate change increases exposure to landslides, floods, and ecosystem degradation, heightening the vulnerability of riverine populations and socioeconomic activities dependent on waterways (Loureiro et al., 2014; Back and Cadorin, 2020; Cavalcante et al., 2020).

Thus, several studies have already been carried out seeking to understand the event of these extreme rains in the country; how-

ever, they are case studies on a local scale and do not usually relate precipitation to other climatological variables, such as air temperature. The study by Regoto et al. (2021) analyzed these variables across Brazil using indexes and trends. However, despite providing important information on the subject, the findings were limited to data from weather stations that are unevenly distributed across the country, and results were spatially represented based on station locations. Additionally, trend analyses were conducted by region rather than by state, making it difficult to assess extreme rainfall behavior on a smaller scale. Even so, this and other studies present evidence of increasing extreme rainfall episodes in different parts of Brazil, especially in the South and Southeast regions. Studies also indicate a trend of rising maximum and minimum temperatures in the country, but it is necessary to investigate whether there is any relation between the increase in these trends, as well as possible geographic patterns, through other data sources with better spatial resolution.

This study aimed to analyze the behavior and evolution of extreme precipitation events in Brazil, identifying possible patterns in their geographical distribution, trends in historical series, and potential correlations with atmospheric temperature trends.

Material and Methods

The methodological approach of this research consisted of the following main steps (Figure 1). First, the study area was defined, encompassing the entire Brazilian territory. Next, the datasets were collected, with the chosen source being the one provided by Xavier et al. (2022). The selected variables for the entire Brazilian territory were precipitation and maximum and minimum temperatures. In the following step, the Climate Extremes Indi-

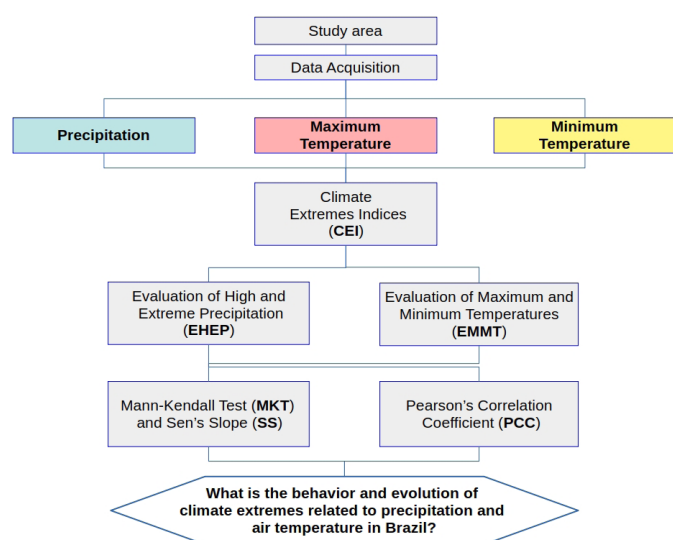


Figure 1 – Flowchart containing the steps necessary to carry out the study.

ces (CEI) were calculated, comprising 11 indices for the Evaluation of High and Extreme Precipitation (EHEP) and 11 for the Evaluation of Maximum and Minimum Temperatures (EMMT). After computing the indices, their trends were analyzed using the Mann-Kendall Test (MKT) and Sen's Slope (SS), along with correlation analyses between some of the indices. Finally, based on the results obtained in the previous steps, the potential implications of the findings were discussed.

Study area

The study area corresponds to the Brazilian territory (Figure 2), the largest country in South America. With a territorial extension of 8.5 million square kilometers, Brazil ranks fifth among the largest countries in the world in terms of area (Brasil, 2022).

The country is divided into five distinct geographic regions: North, Northeast, Midwest, Southeast, and South. Each region has unique characteristics in terms of climate, soil, rainfall, fauna, flora, culture, economy, and topography. Brazil consists of 26 federated states and one Federal District, where the country's capital, Brasília, is located (Cavalcanti, 2016; Brasil, 2022).

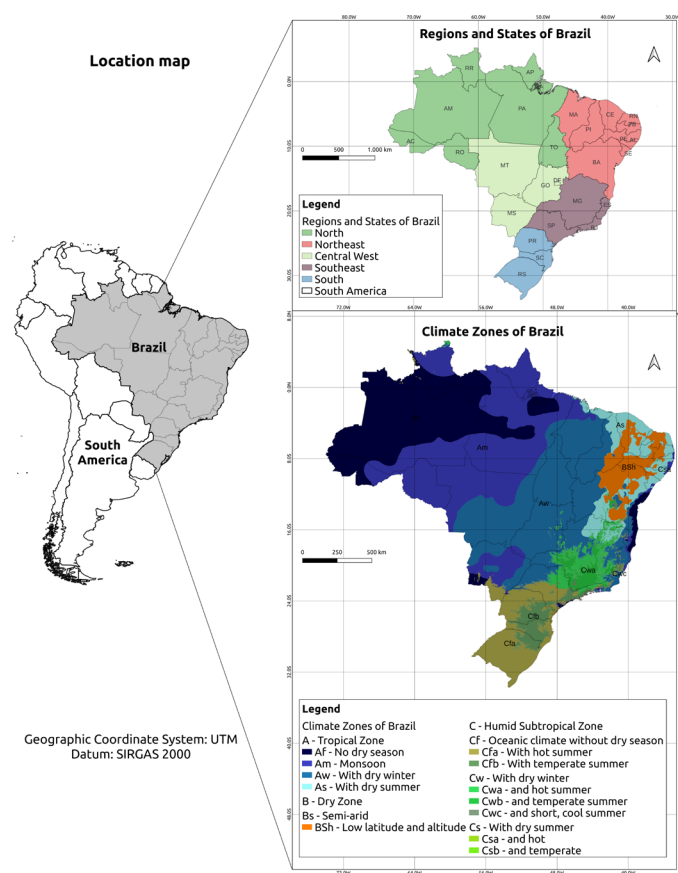


Figure 2 – Location map of the study area.

Source: Shapefile of the Climate Zones of Brazil (Alvares et al., 2013).

Brazil has three main climatic zones: Tropical Zone (A), Dry Zone (B), and Humid Subtropical Zone (C), each with its own subclassifications, totaling 12 climate types (Figure 2), which are defined according to the Köppen system (Köppen, 1936; Peel et al., 2007; Alvares et al., 2013). Further details on this classification can be found in the Supplementary Material.

Data

The Brazilian Daily Weather Gridded Data (BR-DWGD) is a daily-scale meteorological dataset for Brazil [$0.1^\circ \times 0.1^\circ$ resolution], which provides data on precipitation (Pr, mm), maximum and minimum temperatures (Tmax, Tmin: $^\circ\text{C}$), solar radiation (Rs: MJ/m^2), relative humidity (RH: %), wind speed at 2 meters (u2: m/s), and potential evapotranspiration (ETo: mm). The data were compiled by Xavier et al. (2022), and the current time series spans from 1961 to 2022 for Pr, and from 1961 to 2020 for the other meteorological variables.

The variables were gridded through interpolation using observed data from 11,473 rain gauges and 1,252 weather stations

(see details in Xavier et al., 2022). In this study, Pr data from the most recent 32 years available, spanning from 1991 to 2022, were used. The Tmax and Tmin data used correspond to the period from 1991 to 2020 (30 years). This same period was used for Pr when correlating it with temperature.

Extreme precipitation and maximum and minimum temperature evaluation index

At this stage, the CEIs related to EHEP and EMMT were adopted, applied to the entire Brazilian territory, according to studies proposed and applied in different regions of the world, such as: Manton et al. (2001); Griffiths et al. (2003); Haylock et al. (2006); Hountondji et al. (2011); Donat et al. (2013); Berhane et al. (2020); Bhatti et al. (2020); Cavalcante et al. (2020); Regoto et al. (2021); Yaduvanshi et al. (2021); Yao et al. (2021); Zhu et al. (2022). Table 1 shows these indices, as well as their acronyms, definitions, and units of measurement used for each analysis.

Table 1 – Indexes of climatic extremes, with their acronyms, definitions, and units.

Acronym	Name	Definition	Unit
Precipitation			
1) TOTPR	Total Precipitation	Accumulated annual rainfall	(mm/year)
2) DPR	Days with Precipitation	Annual total rainy days (A rainy day has rainfall ≥ 1 mm)	(days/year)
3) SDII	Simple Daily Intensity Index	Average rainfall on rainy days	(mm/day)
4) MAXPR-1D	Maximum Rainfall in 1 Day	Maximum rainfall occurred in just 1 day	(mm/day)
5) MAXPR-5D	Maximum Precipitation in 5 Days	Maximum accumulated rainfall in 5 consecutive days	(mm/5 days)
6) FDHR-P95	Frequency of Days with High Rainfall (P95)	Annual count of days with precipitation $\geq 95^{\text{th}}$ percentile	(days/year)
7) FDER-P99	Frequency of Days with Extreme Rainfall (P99)	Annual count of days with precipitation $\geq 99^{\text{th}}$ percentile	(days/year)
8) IDHR-P95	Intensity of Days with High Rainfall (P95)	Cumulative annual rainfall of rainy days $\geq 95^{\text{th}}$ percentile	(mm/year)
9) IDER-P99	Intensity of Days with Extreme Rainfall (P99)	Cumulative annual rainfall of days with rain $\geq 99^{\text{th}}$ percentile	(mm/year)
10) PDHR-P95	Proportion of Days with High Rainfall (P95)	Percentage of total annual days with precipitation $\geq 95^{\text{th}}$ percentile	(%)
11) PDER-P99	Proportion of Days with Extreme Rainfall (P99)	Percentage of total annual days with precipitation $\geq 99^{\text{th}}$ percentile	(%)
Maximum and Minimum Temperatures			
1)TX-M	Average Maximum Temperature (TX)	Annual average between daily maximum temperatures	($^\circ\text{C}/\text{year}$)
2)TN-M	Average Minimum Temperature (TN)	Annual average between daily minimum temperatures	($^\circ\text{C}/\text{year}$)
3) DTA	Daily Thermal Amplitude	Annual average between maximum and minimum daily temperature differences	($^\circ\text{C}/\text{year}$)
4) TX-X	Maximum TX	Maximum annual value of TX	($^\circ\text{C}$)
5) TN-X	Maximum TN	Maximum annual value of TN	($^\circ\text{C}$)
6) TX-N	Minimum TX	Minimum annual value of TX	($^\circ\text{C}$)
7) TN-N	Minimum TN	Minimum annual value of TN	($^\circ\text{C}$)
8) TX-P10	Cold days	Percentage of days per year with TX \leq percentile 10	(%)
9) TN-P10	Cold nights	Percentage of days per year with TN \leq percentile 10	(%)
10) TX-P90	Hot days	Percentage of days per year with TX \geq percentile 90	(%)
11) TN-P90	Hot nights	Percentage of days per year with TN \geq percentile 90	(%)

Annual total precipitation, days with annual precipitation and simple daily intensity index

The total annual accumulated precipitation (TOTPR) was obtained by averaging the accumulated precipitation values for each year analyzed. In other words, the climatology for each region of the country was carried out to understand the spatial distribution of rainfall across the entire study area.

The days with annual precipitation (DPRs) were calculated by counting the annual number of days considered rainy (rainfall greater than or equal to 1 mm). This means that any day without rainfall, or with minimal rainfall (below 1 mm), was excluded from this count. Afterward, the annual average was calculated using the values obtained from the count for each year in the analyzed historical series.

The SDII was calculated by quantifying the DPRs obtained from the previous metric, and based on them, the daily average of precipitation that occurred on these rainy days was determined. It was also possible to find the average rainfall intensity, expressed in millimeters per day.

Maximum precipitation at one day and five days

The maximum precipitation at one day (MAXPR-1D) metric verified the maximum daily rainfall that occurred in the analyzed historical period. Thus, it was possible to obtain the maximum daily rainfall volume and observe the areas with the highest and lowest impact based on their respective maximums.

MAXPR-5D analyzes the maximum accumulated rainfall that occurred on the next five consecutive days. In other words, the total precipitation volumes were summed up every five days, with overlap. The precipitation from the first to the fifth day was summed first, then from the second to the sixth day, and so on. At the end of this process, performed on all days within the selected historical series, the highest five-day total was found, and this became the maximum precipitation at five days (PRMAX-5D).

Frequency, intensity and proportion of days with high or extreme rainfall

The other EHEP indexes (6-11), which are FDHR-P95, FDER-P99, IDHR-P95, IDER-P99, PDHR-P95, PDER-P99, are related to the precipitation percentiles obtained from the historical series. First, these percentiles were generated by classifying the respective DPR data in ascending order, which were then divided into hundredths (each part representing 1% of the data) and are denoted as P1, P2, ..., P100. Based on this, the P95 and P99 were calculated, which, according to Manton et al. (2001), are related to high and extreme rainfall, respectively.

After obtaining the 95th and 99th percentiles, these were applied to the indexes mentioned in this section. FDHR-P95 was calculated as the average of the number of annual days with daily precipitation equal to or greater than P95, while the FDER-P99 used the same calculation but applied to P99. The IDHR-P95 and IDER-P99 also considered rainfall

equal to or above their respective percentiles. However, this time, the sum of the precipitated values for each year in the data series was calculated, followed by the subsequent average of the annual accumulations. Finally, PDHR-95 and PDHR-99 were determined by the ratio between the annual accumulated volume of precipitation that was equal to or greater than the 95th and 99th percentiles, respectively, and the total annual accumulated rainfall in the same year. So it is the average (or proportion) between high ($\geq P95$) or extreme ($\geq P99$) rainfall and the total precipitation in a given year. The average of these annual sums was then calculated.

Maximum average and minimum average temperatures and daily thermal amplitude

The average maximum temperature (TX-M) metric was obtained through the simple annual average between the daily values of maximum temperature. The same logic was applied to the average minimum temperature (TN-M) metric, which was obtained through the simple annual average between the daily minimum temperature data.

The daily thermal amplitude (DTA), however, relates the daily maximum and minimum temperature data by calculating the difference between their values, thus obtaining the daily temperature variation over the proposed period. After that, the annual average of these daily temperature ranges was calculated for each year. Finally, the annual averages (for all years) for each of the three indices mentioned in this section were calculated.

Maximum Maximum Temperature, Maximum Minimum Temperature, Minimum Maximum Temperature and Minimum Minimum Temperature

These four indices follow the same premise, which is to assess the extremes, both higher and lower, for each type of temperature analyzed. For each metric, the extremes were obtained within the proposed historical period as follows: the maximum temperature among the daily maximum temperatures (TX-X); the maximum temperature among the daily minimum temperatures (TN-X); the minimum temperature among the daily maximum temperatures (TX-N); the minimum temperature among the daily minimum temperatures (TN-N).

Cold days, cold nights, hot days and hot nights

TX-P10 and TN-P10 are indices that relate to the coldest days and nights over a given year, respectively. They were obtained by quantifying the days when the daily maximum and minimum temperatures were less than or equal to the 10th percentile ($\leq P10$). On the other hand, TX-P90 and TN-P90 were the indices used to detect the hottest days and nights in each analyzed year, respectively, and they were measured by quantifying the days when the daily maximum and minimum temperatures were higher than or equal to the 90th percentile ($\geq P90$).

Trend analysis: Mann-Kendall Test and Sen's Slope

Trend analysis was performed for all EHEP and EMMT indexes, using the Mann-Kendall Test (MKT), along with Sen's Slope (SS). According to Yue and Wang (2004), the application of the Mann-Kendall Test statistic to a sample of "n" random variables, independent and distributed identically, is performed by Equations 1 and 2:

$$S = \sum_{i=1}^{n-1} \sum_{j=i+1}^n \text{sgn}(X_j - X_i) \quad (1)$$

Where S = the time series values at equal time intervals;
i and j = the time index;
n = number of time series elements. And:

$$\text{sgn}(X_j - X_i) = \begin{cases} +1 & \text{if } (X_j - X_i) > 0; \\ 0 & \text{if } (X_j - X_i) = 0; \\ -1 & \text{if } (X_j - X_i) < 0 \end{cases} \quad (2)$$

According to the null hypothesis test (Ho), which assumes no trend, this is valid for the Mann-Kendall Test when the p-values are lower than the critical values (called alpha)—in this case alpha=0.05 (used to obtain a significance level of 95%); that is, when $p < \alpha$, the time series has no trend. Otherwise, if the $p \geq \alpha$, the time series has a trend. Further details can be found in Yue and Wang (2004). The Python data used was "pymannkendall".

The Sen estimator (Q) is generally used as a complement to the Mann-Kendall Test. This estimator provides the magnitude of detected trends. According to Sen (1968), this value is estimated using Equation 3:

$$Q_{ij} = \frac{X_j - X_i}{j - i}, \text{ with } i < j \quad (3)$$

Where "Xi" and "Xj" are related to the values of the variable under study at the "i" and "j".

Positive values of Q indicate an increasing trend and negative values indicate a decreasing trend. By analyzing the temporal order of the data, the test examines whether the observations show consistent patterns over time, without assuming a specific distribution of the data (Sen, 1968). The test results indicate whether there is sufficient statistical evidence for the presence or absence of a significant trend. If the test shows statistical significance, this suggests that there is a systematic change in observations over time, which helps to understand patterns of variability and changes in time series, such as those related to climate or the environment (Hirsch et al., 1982).

Pearson correlation coefficient

Pearson's Correlation Coefficient (PCC) is a statistical metric that measures the strength and direction of a linear relationship between two random variables. Historically, it is the first formal measure of cor-

relation and is still one of the most widely used (Zhou et al., 2016). The PCC of two variables X and Y is formally defined as the covariance between these two variables (which indicates the level at which they vary together) divided by the product of their standard deviations (which acts as a normalization factor), and can be defined equivalently by Equation 4:

$$r_{xy} = \frac{\sum (x_i - \bar{x}) \sum (y_i - \bar{y})}{\sqrt{\sum (x_i - \bar{x})^2} \sqrt{\sum (y_i - \bar{y})^2}} \quad (4)$$

Where $\bar{x} = \frac{1}{n} \sum_{i=1}^n x_i$ denotes the average of x;

$\bar{y} = \frac{1}{n} \sum_{i=1}^n y_i$ denotes the average of y;

the coefficient r_{xy} ranges from -1 to 1 and is invariant to the linear transformations of any of the variables.

Thus, it is possible to identify whether the variables are positive, negative or uncorrelated, in a range from +1 (directly related) to -1 (inversely related), with 0 denoting the absence of relationship between the variables, respectively (Adler and Parmryd, 2010). In this study, the "numpy.corrcoef" function was used, which returns Pearson's product-moment correlation coefficients, belonging to the Python programming language. Correlations were made between cumulative annual rainfall data (total, high [$\geq p95$] and extreme [$\geq p99$]), and annual averages of maximum and minimum temperatures. For the analysis of correlations, the classification defined by Hinkle et al. (2003) was used, according to Table 2.

Table 2 – Practical rule for interpretation of the correlation coefficient interval.

Correlation Range	Interpretation
± 0.9 to ± 1.0 (< -0.9 or > 0.9)	Very high
± 0.7 to ± 0.9 (-0.7 to -0.9 or 0.7 to 0.9)	High
± 0.5 to ± 0.7 (-0.5 to -0.7 or 0.5 to 0.7)	Moderate
± 0.3 to ± 0.5 (-0.3 to -0.5 or 0.3 to 0.5)	Low
± 0.0 to ± 0.3 (-0.3 to 0.3)	Very low

Results

Evaluation of high and extreme precipitation and its tendencies

Total precipitation and simple daily intensity index

The mean values of TOTPR are presented in Figure 3A. The North region exhibits the highest annual precipitation totals, whereas the Northeast presents the lowest. Figure 3B suggests a positive trend across much of the North region and a negative trend in parts of the Center-West and different areas of the Southeast. The results for TOTPR and DPR were spatially similar; therefore, DPR has been included in the Supplementary Material.

The Simple Daily Intensity Index (SDII) (Figure 3C) indicates that the regions with the lowest and highest daily precipitation values are the Northeast and South, respectively. The corresponding SS for ISID is presented in Figure 3D and shows a positive trend mainly in the North and South regions. The Northeast and Center-West display both positive and negative trend areas; however, areas with negative trends prevail. Further details regarding the results of Figures 3A-3D can be found in the Supplementary Material.

Maximum precipitation in 1 day and maximum precipitation in 5 days

MAXPR-1D is shown in Figure 4A. The results indicate that most of the Brazilian territory experienced maximum daily rainfall values ranging between 50 mm/day and 125 mm/day. The South region generally exhibited the highest values. The SS associated with MAXPR-1D (Figure 4B) shows that most states displayed positive trends across various areas of their territories, while negative trends were more concentrated in the Center-West and Southeast regions.

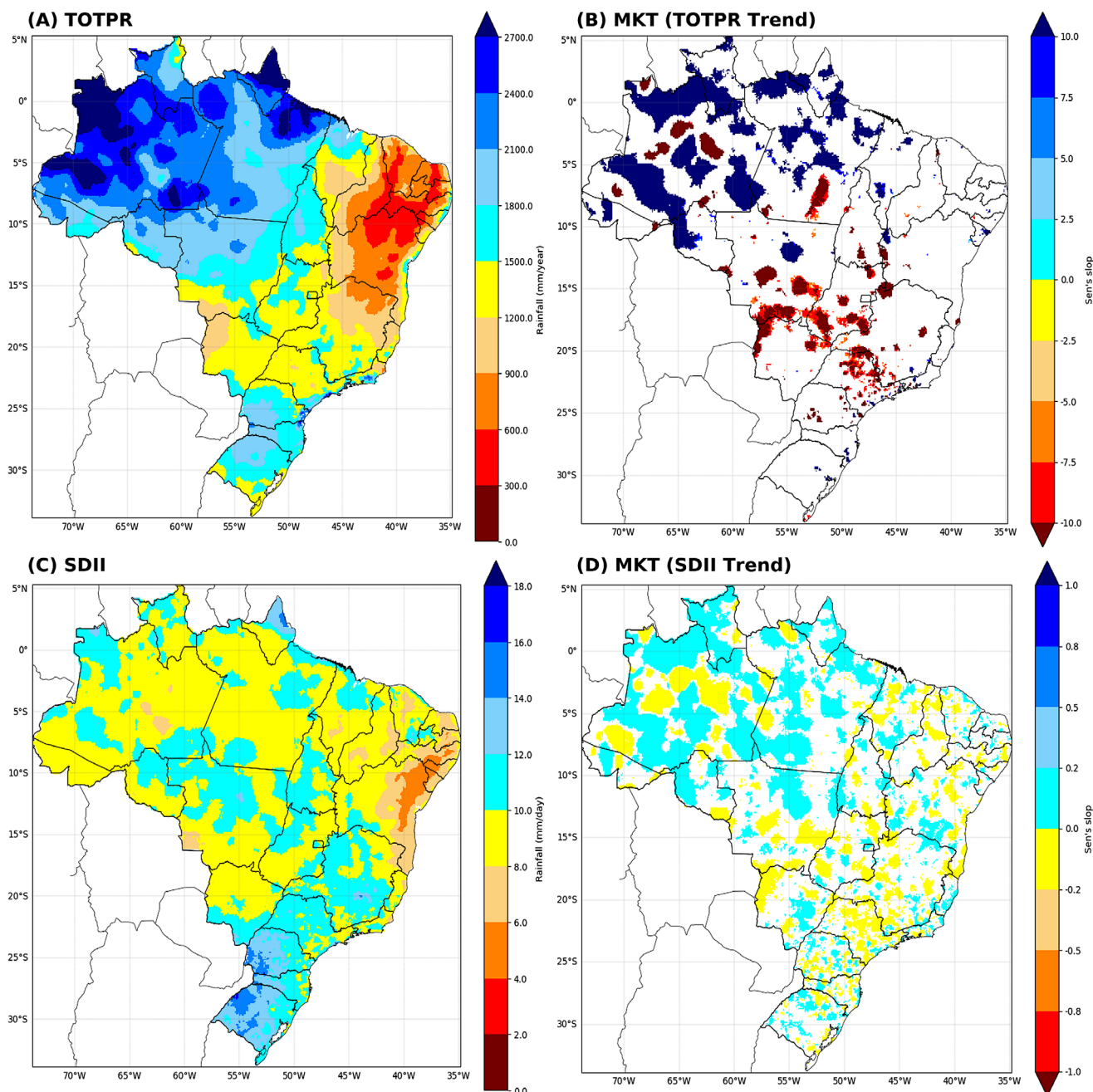


Figure 3 – Map of Brazil containing: (A) Total Precipitation (TOTPR); (B) TOTPR Trend; (C) Simple Daily Intensity Index (SDII); (D) SDII Trend. The white color indicates no trend.

MAXPR-5D (Figure 4C) shows that the maximum 5-day rainfall was lower in almost the entire Northeast, while the Southeast and South were the regions with the highest aggregate values. The SS shown in Figure 4D indicates an increase in these consecutive rainfall events in almost the entire country, with negative trends observed mainly in large parts of the North, some coastal areas of the Northeast, and a few locations in the Southeast and South. Further details regarding the results for this index can be found in the Supplementary Material.

Proportion of days with high rainfall and proportion of days with extreme rainfall

The proportion of days with high rainfall (PDHR-P95) is shown in Figure 5A. The results suggest that the states in the North and Center-West regions exhibit the lowest percentage indices. The South, in general, recorded the highest average percentage, with almost its entire territory showing values above 21%. The SS obtained for annual PDHR-P95 (Figure 5B) indicates an increasing trend in the North, Northeast, and South regions, whereas the Center-West and Southeast regions exhibit a decreasing trend.

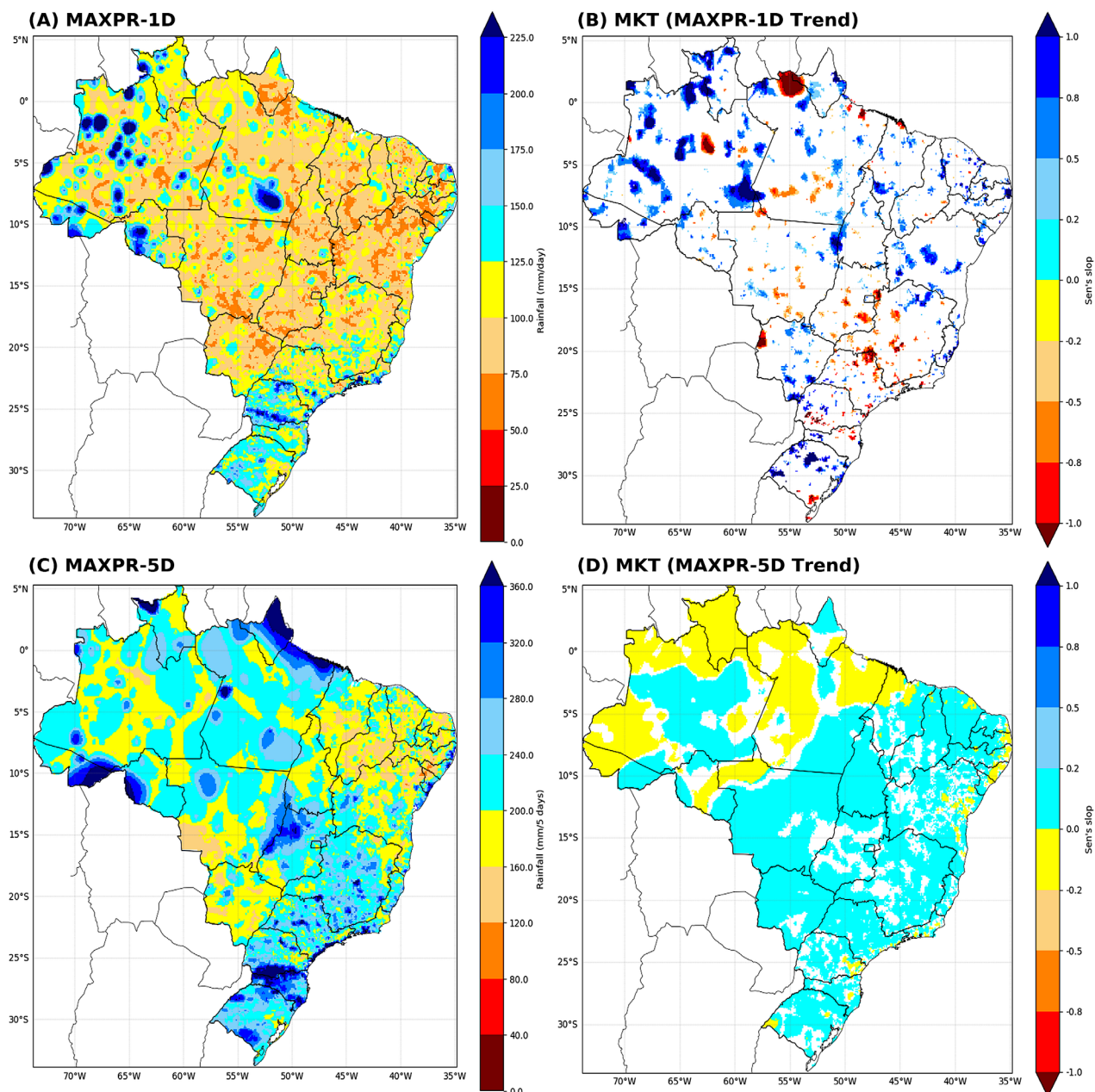


Figure 4 – Map of Brazil containing: (A) Maximum Precipitation in 1 day (MAXPR-1D); (B) MAXPR-1D Trend; (C) Maximum Precipitation in 5 days (MAXPR-5D); (D) MAXPR-5D Trend. The white color indicates no trend.

Figure 5C shows the proportion of days with extreme rainfall (PDER-P99). The South region recorded, in general, the highest average percentage. The SS of the PDER-P99 (Figure 5D) shows that most of the country exhibits positive trends, with higher frequency in the North, Northeast, and South regions. Negative trends were mostly detected in portions of the states of Pará, Goiás, Minas Gerais, and São Paulo.

Further details of the results of these indexes can be found in the Supplementary Material. The results between FDHR-P95, IDHR-P95, and FDER-P99, IDER-P99, were spatially similar to those of PDHR-P95 and PDER-P99, respectively, mainly regarding SS maps. Consequently, these results have also been included in the Supplementary Material.

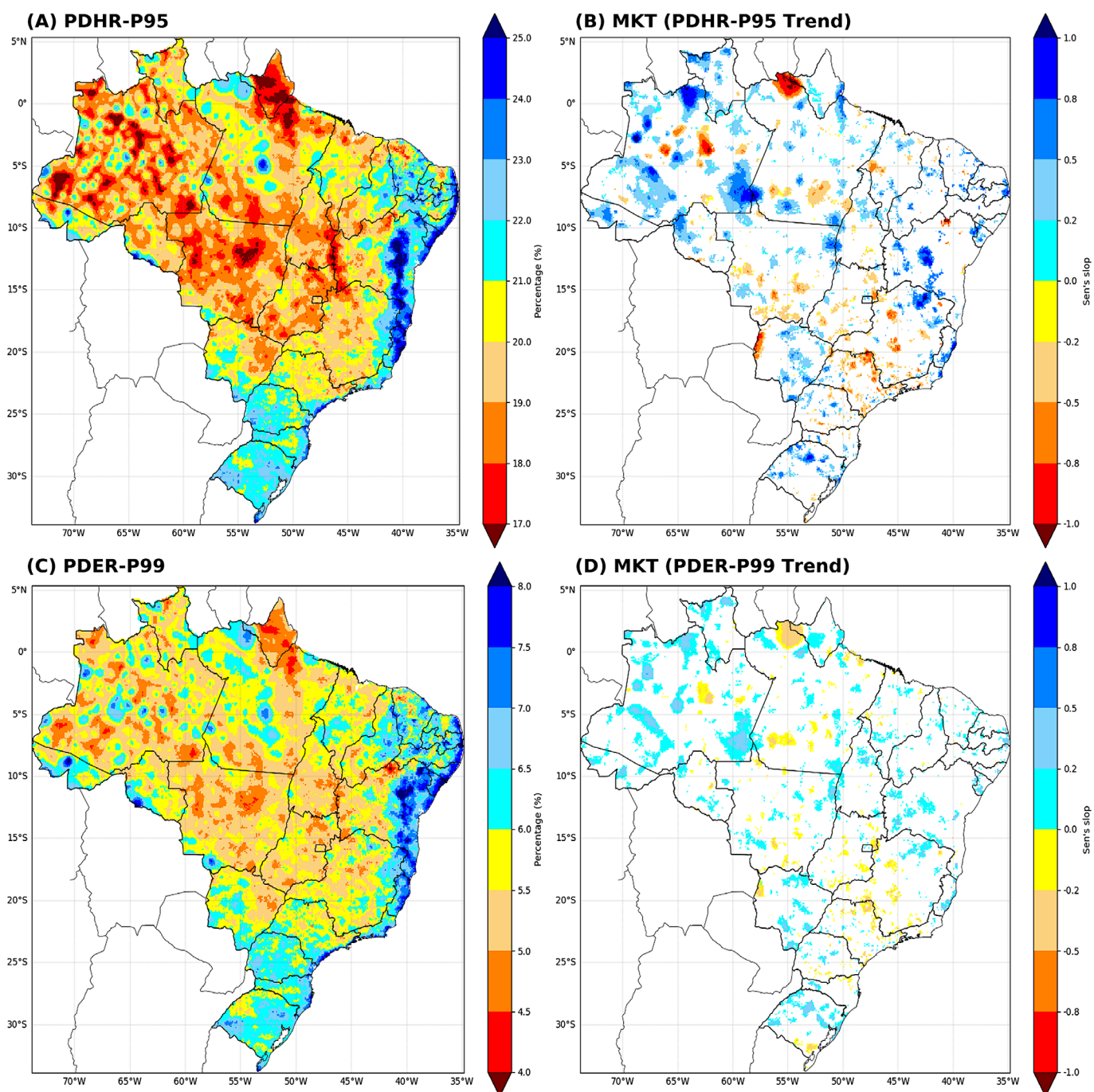


Figure 5 – Map of Brazil containing: (A) Proportion of Days with High Rainfall ($\geq P95$) (PDHR-P95); (B) Trend of PDHR-P95; (C) Proportion of Days with Extreme Rainfall ($\geq P99$) (PDER-P99); (D) Trend of PDER-P99. The white color indicates no trend.

Evaluation of maximum and minimum temperatures and its trends

Average maximum temperature, average minimum temperature and daily thermal amplitude

The TX-M, depicted in Figure 6A, indicates that the highest maximum temperatures occur in the North, Northeast, and Center-West regions. The SS for TX-M, shown in Figure 6B, suggests a positive trend across most of Brazil, especially in the Northeast. The TN-M, presented in Figure 6C, shows that the highest minimum temperatures are found in the North and Northeast regions, while the other regions have milder temperatures, especially in the South. Figure 6D displays the DS, which indicates an increasing trend in TN-M across the entire North region, much of the Northeast, Center-West, and Southeast. Figure 6E illustrates the DTA, which was lower in coastal regions throughout Brazil. The highest DTAs were recorded in the more central parts of the country. In Figure 6F, the SS obtained for DTAs indicates a positive trend in the Northeast and Center-West, a negative trend in the North and Southeast, and mixed signals in the South.

Further details on the description of the results of these indexes can be found in the Supplementary Material. The results for TX-X, TN-X, TX-N, TN-N, TX-P10, TN-P10, TX-P90 and TN-P90 were spatially similar to those of TX-M, TN-M and DTA, showing an overall increase in both maximum and minimum temperatures across most of the country. These results are also available in the Supplementary Material.

Correlation and comparison of trends between evaluation of high and extreme precipitation and evaluation of maximum and minimum temperatures

The first correlation was conducted between TOTPR and TX-M (Figure 7A), showing a negative correlation across most of the country, indicating an inverse interdependence between these variables. The North region exhibited both negative and positive correlations more frequently than other regions. The second analysis examined the correlation between TOTPR and TN-M (Figure 7B), with results suggesting stronger negative correlations in parts of the Northeast. The South was the region with the most positive correlation values overall.

Additionally, the correlation between TX-M and precipitation events greater than or equal to the 95th percentile ($\geq P95$) was calculated (Figure 7C), covering the FDHR-P95, IDHR-P95 and PDHR-P95 indexes. The most positive correlations (ranging between 0.4 and 0.8, classified as low to high) were more frequent in the states of Amazonas and Rondônia. Meanwhile, negative correlations (ranging between -0.4 and -0.8) were more prevalent in parts of the Northeast. The correlation between TN-M and precipitation events related to P95 (Figure 7D) indicates a positive correlation in the South of the country, with values ranging from 0.6 to 0.8 (classified as moderate to high). Conversely, negative correlations were more prominent in parts of Amazonas state, also classified as moderate to high.

Further details on these PCCs results can be found in the Supplementary Material. The correlations between TX-M and TN-M with P99 were spatially similar to those with P95, differing only in the correlation scale, which was lower. Therefore, these results were also included in the Supplementary Material.

The PCCs indicated whether climate variables were directly or inversely interdependent, but the SS results reveal which of these variables showed increasing or decreasing trends. To enhance understanding, Figures 8A-8D was created using the same method as Figure 7 but comparing trends instead of correlations. Our results suggest that the Northern region exhibited the most compatible trends, particularly those related to the increase in maximum/minimum temperatures and extreme rainfall. The Northeast and South regions showed fewer trend relationships between PRTOT and TX-M/TN-M. However, this changes when $PR(\geq P95)$ is related to these temperature indices, revealing several locations with positive trends for both climate variables, especially near the coastal areas.

In the Center-West and Southeast, specifically in states Mato Grosso, Goiás, Minas Gerais, and the central-northern part of São Paulo, trends indicated decreasing precipitation and increasing temperatures. Only in Figure 8B was there a positive trend for TOTPR and a negative trend for TN-M in these states. Meanwhile, in Mato Grosso do Sul and along the coastal areas between São Paulo and Espírito Santo, there were combined trends of increasing heavy rainfall and rising maximum and minimum air temperatures (Figures 8C and 8D).

Discussion

Based on the presented results, there is a noticeable trend of increasing extreme rainfall in the South region and parts of the North and Northeast, specifically along the northeastern coast, in Sergipe, portions of Bahia, and the Southeast coast. At the same time, there is a decreasing trend in precipitation in the Central-West and Southeast regions, and to a lesser extent in the North. Chagas et al. (2022) described the performance of satellite products for extreme rainfall events that triggered natural disasters across various climatic regimes in Brazil, indicating that Mesoscale Convective Systems (MCS) accounted for over 90% of extreme rainfall in the South and about 60 to 90% of extreme rainfall in the Northeast. Extreme droughts in the North and Northeast, along with extreme rainfall and flooding in the South, also reflect the impacts of the El Niño-Southern Oscillation (ENSO), a meteorological phenomenon affecting the Equatorial Pacific Ocean and causing climate variations worldwide, including in Brazil (Philander, 1998; Yeh et al., 2009). However, other climatic factors may also be associated with these extreme events in the specified regions, as well as in other areas of the country, leading to an increase in both the frequency and intensity of extreme rainfall.

By understanding the role of air temperature and its influence on the hydrological cycle, the atmosphere, and consequently, cloud and rainfall formation, it is possible to perceive that changes in the climate of a region can bring significant impacts and changes

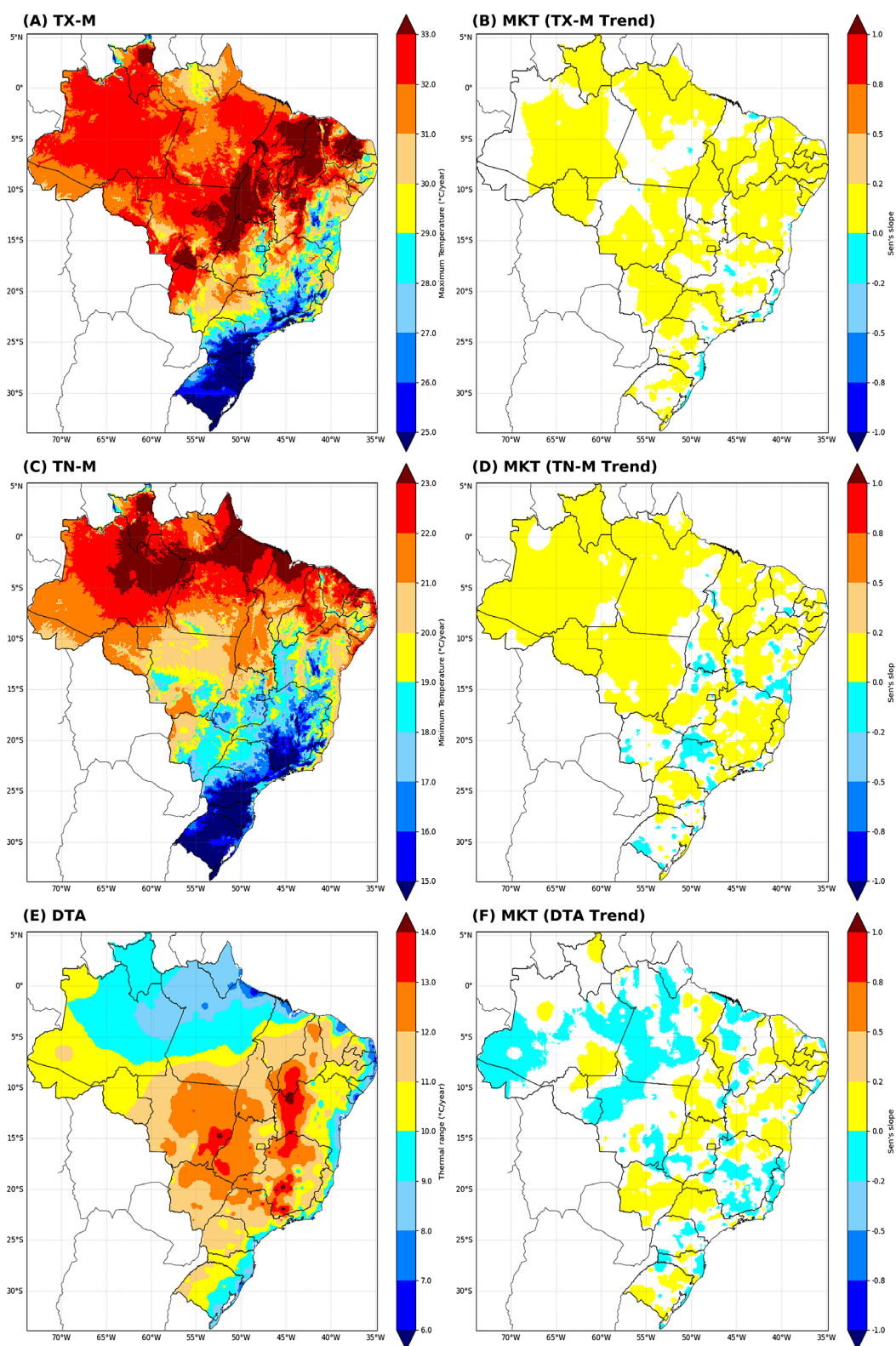


Figure 6 – Map of Brazil containing: (A) Maximum Temperature (TX) Average (TX-M); (B) TX-M Trend; (C) Minimum Temperature (TN) Average (TN-M); (D) TN-M Trend; (E) Daily Thermal Amplitude (DTA); (F) DTA Trend. The white color indicates no trend.

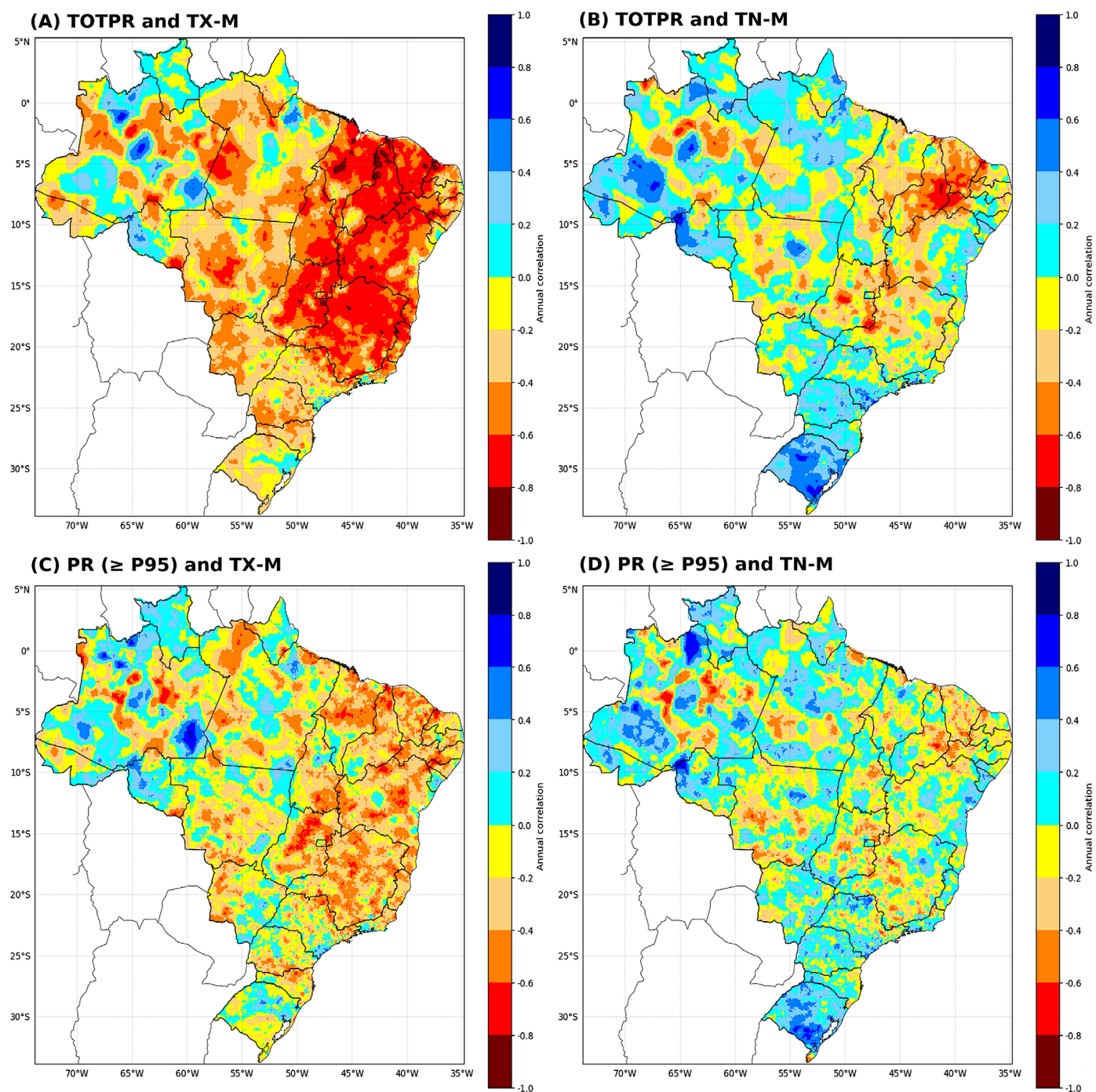


Figure 7 – Map of Brazil containing: (A) Correlation between TOTPR and TX-M; (B) Correlation between TOTPR and TN-M; (C) Correlation between PR ($\geq p95$) and TX-M; (D) Correlation between PR ($\geq p95$) and TN-M.

in the climate structure, not only at the local scale but also at the regional, national, and global scales. The increase in atmospheric temperatures compared to the pre-industrial period (1850–1900), as indicated by the Intergovernmental Panel on Climate Change (IPCC), shows a global average rise of $+1.09^{\circ}\text{C}$ in the recent period (2011–2020), according to its Sixth Assessment Report (AR6).

Projections estimate temperatures of $+1$ to $+1.8^{\circ}\text{C}$ by the end of the century (2081–2100) under the best emissions scenario and $+3.3$ to $+5.7^{\circ}\text{C}$ under the worst scenario (IPCC, 2023). The results of this study also indicate a trend of increasing maximum temperatures (TX-M) across Brazil, as well as minimum temperatures (TN-M), albeit to a lesser extent in Mato Grosso do Sul, São Paulo, Santa Ca-

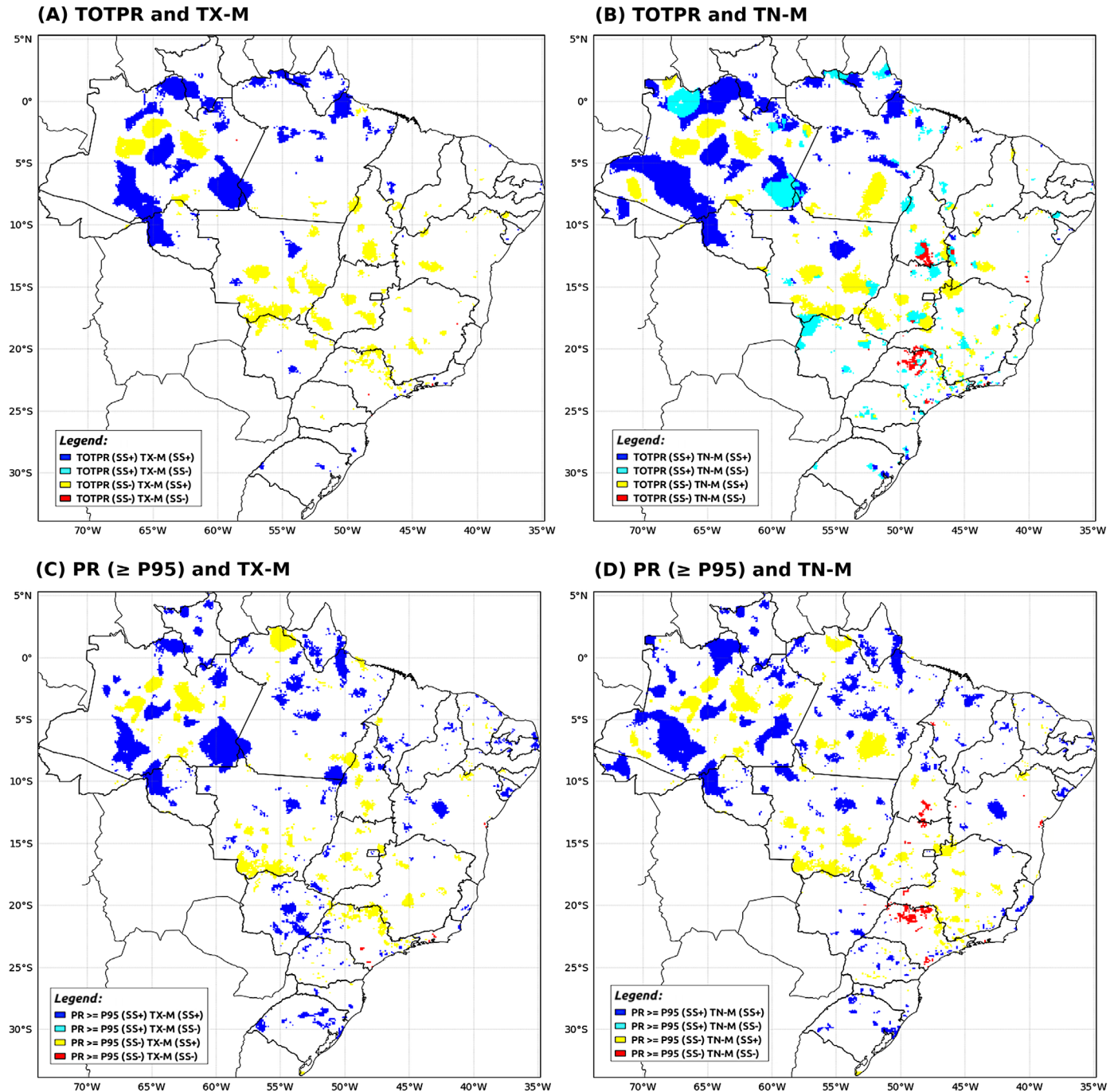


Figure 8 – Map of Brazil containing trend comparisons: (A) TOTPR and TX-M; (B) TOTPR and TN-M; (C) PR ($\geq p95$) and TX-M; (D) PR ($\geq p95$) and TN-M. The white color indicates non-combination between trends.

tarina, and Rio Grande do Sul. Additionally, there is an observed increase in hot days and nights (TX-P90 and TN-P90) and a decrease in cold days and nights (TX-P10 and TN-P10), findings consistent with those reported by da Silva et al. (2019) and Costa et al. (2020).

Such an increase in temperatures may cause permanent damage, as in the case of the Amazon Rainforest, for example.

According to the study by Flores et al. (2024), there is a possibility that the Amazon forest system could soon reach a tipping point due to the unprecedented stress it has been experiencing, caused by rising temperatures, extreme droughts, deforestation, and fires, even in central and remote parts of the system. The authors estimated that, by 2050, between 10 and 47% of the forests in the Amazon could be exposed

to compositional disturbances, triggering unexpected ecosystem transitions and potentially exacerbating regional climate change. This is concerning, as rainfall regimes in Brazil also depend on the Amazon, which emits large amounts of humid air resulting from plant evapotranspiration. This moisture is drawn by suction into the trade winds from the Atlantic Ocean and transported into the continent, generating the so-called “flying rivers” (Paiva and Prezoto, 2021). The disruption of this system could lead to an imbalance in rainfall across the country, particularly in the Southeast and South, as, according to Fisch et al. (1998) and Clement and Higuchi (2006), the Amazon is responsible for 25–50% of the rainfall in the Southeast and also exerts a strong influence on rainfall in the South.

To better investigate this interaction, trend analyses were conducted using MKT and SS, and PCCs. The PCCs showed a stronger negative correlation in the Northeast and Southeast, followed by the Central-West region (TOTPR/PR-P95 and TX-M). When analyzing the DSSs, it was observed that maximum temperature shows an increasing trend, while precipitation exhibits a decreasing trend, particularly in the Southeast and Central-West regions. In the Northeast, no significant trends were detected for most EHEP indexes, and in some areas there was even a trend of increasing extreme rainfall. On the other hand, SDII showed a positive trend in some locations where DPR had a negative trend, indicating an increase in intensity and a decrease in frequency and a reduction in MAXPR-5D in parts of its coastline. The results obtained in this study align with those of Costa et al. (2020), which did not report statistically significant trends for most EHEP indexes. Similarly, Carvalho et al. (2019) identified a decreasing trend in the number of rainy days along the northeastern coast, as well as a rising temperature trend in inland regions. In the South, a significant positive correlation was found only in a small area between the central-northern part of Rio Grande do Sul, where both maximum temperature and extreme rainfall exhibited a positive trend.

Significant PCCs (>0.5) between TOTPR/PR-P95 and TN-M were negative in the Northeast (central-northern portion), Central-West, and Southeast (specifically in the states of Goiás and Minas Gerais). In contrast, they were positive in the South (mainly in Rio Grande do Sul) and exhibited both positive and negative values in the North (notably in Amazonas and Rondônia). The SSs indicated an increase in minimum temperatures in the specified northeastern region, though this was not necessarily accompanied by a decrease in precipitation despite the high negative correlation in this area. In the Central-West and Southeast, there was a clear trend of rising minimum temperatures, along with areas showing a decreasing trend in precipitation. For example, in the Federal District, no increasing trend in extreme rainfall was observed, a finding also reported by Silva and da Franca (2021). However, in São Paulo’s metropolitan region, the results suggest a rising trend in extreme rainfall. Marengo et al. (2020) similarly identified a significant increase in total precipitation during the rainy season over

the past seven decades. In the 1950s, heavy rainfall events (exceeding 50 mm) were absent, whereas, in the past ten years, such events have occurred two to five times annually. This, combined with inadequate land use in risk-prone areas, such as riverbanks and hillsides, has contributed to flooding, inundations, and landslides.

In the North, given that there are both positive and negative significant correlations and that temperatures are trending upward, most of these correlations align with precipitation trends. In the South, there is a strong increasing trend in heavy and extreme rainfall across nearly all EHEP indexes for different regions of Rio Grande do Sul. Additionally, there is a high positive correlation between these extreme rainfall events and minimum temperature, particularly in the southern part of the state. However, there are almost no significant trends for TN-M. Where such trends do exist (in the northern and eastern portions of the state), there is also an increasing trend in heavy and extreme rainfall. This suggests that if, in the future, minimum temperature trends increase in the southernmost part of Rio Grande do Sul, there may be a corresponding rise in extreme rainfall in this region. Furthermore, there is the potential for the North, with rising temperatures, to generate even more humid air, which could be transported by atmospheric circulation. This moisture may be directed by the Andes Mountains toward southern Brazil (Portella et al., 2022), potentially causing more extreme rainfall events in the region.

The study by Regoto et al. (2021) presents similar findings, showing an increase in hot extremes and a decrease in cold extremes, indicating widespread and consistent warming across Brazil. It also identified an increasing trend in extreme rainfall in the South while detecting a decreasing trend in the Northeast. However, in the present study, the latter result diverged, as there was little significant trend in elevated and extreme rainfall for the Northeast, and where trends did appear, they were mostly positive. This discrepancy may be related to differences in the years selected for analysis, the type of data used, the methodology applied in data processing, or even the lack of significant variation in annual rainfall totals over the past three decades. The Northeast has experienced severe droughts for centuries, has low yearly precipitation totals, and is already undergoing desertification in some areas, such as parts of Bahia (da Costa et al., 2018; Montenegro, 2023). Even if rainfall decreases further, these variations tend to be small due to the region’s persistent water deficit, making them difficult to detect using MKT and SS analyses.

It is also important to highlight that in a semi-arid region like the Brazilian Northeast, there may be a decreasing trend in total annual precipitation while still observing an increasing trend in extreme rainfall events, as shown in the present study, which aligns with the findings of da Silva et al. (2019) and Costa et al. (2020). Regoto et al. (2021) also considered that, with the intensification of temperature extremes, the effects of El Niño-Southern Oscillation (ENSO) could become more pronounced, further exacerbating conditions in regions already affected by this climatic phenomenon. In the South, increased convection

would occur, while the opposite effect would be observed in the North-east. This would influence the positioning of the Intertropical Convergence Zone (ITCZ), shifting it further into the Northern Hemisphere and creating a more drought-prone scenario in the Brazilian Northeast. Simultaneously, the South Atlantic Convergence Zone (SACZ) would be displaced further into the Southern Hemisphere, contributing to wetter conditions in southern Brazil (Haylock et al., 2006).

Conclusion

In general, the results of this study indicated a trend of increasing average maximum and minimum temperatures across most of Brazil, along with a rise in hot days and nights and a decrease in cold days and nights. The trends and correlations between precipitation and temperature revealed a reduction in extreme rainfall in the Central-West, Southeast, and parts of the North, while extreme precipitation increased in the South and North, as well as in parts of the Northeast and Southeast, with a greater concentration along their coastal areas. This pattern may suggest a potential increase in atmospheric moisture due to rising temperatures, with this moisture being transported to other regions of the country through atmospheric circulation. As a result, cloud formation could intensify, leading to more frequent extreme rainfall events both in areas experiencing temperature increases and in regions receiving transported humidity.

The climate phenomena MCS and ENSO, which are active in Brazil, already contribute to the occurrence of extreme rainfall events.

However, as seen in the results of this study, there is a probable change underway in the country's climate, which may be related to global climate change, mainly due to greenhouse gas (GHG) emissions, as pointed out in the IPCC AR6 (IPCC, 2023). This may be significantly contributing to the increasing frequency, distribution, and intensity of extreme precipitation events, which should be further investigated in future studies. Densely populated areas are more affected by these extreme events due to high concentrations of pollutants that enhance condensation processes, the formation of urban heat islands, increased surface runoff due to reduced soil infiltration, and improper land use and occupation. These factors collectively exacerbate flooding, inundations, and even desertification in certain regions.

Therefore, it is crucial to implement adaptation strategies such as strengthening early warning systems, investing in resilient infrastructure, protecting aquifer recharge areas, and promoting environmental conservation efforts. These measures are essential to address the growing challenges posed by extreme precipitation events across all regions of Brazil.

Acknowledgements

To UFC, LRH, the MODELHI research group and the coordination of the POSDEHA program for the institutional support. To CAPES for the granting of scientific research resource, and the financial support of the projects: FUNCAP, Process: PS1-0186-00326.01.00/21 and CNPq, Process: 306380/2023-4.

Author's Contributions

Costa, J.M.F.: data curation, formal analysis, investigation, methodology, software, writing – original draft, writing – review & editing. **Marcos Junior, A.D.:** data curation, formal analysis, methodology, software, validation, writing – review & editing. **Gonçalves, S.T.N.:** investigation, validation, writing – original draft writing – review & editing. **Silveira, C.S.:** conceptualization, funding, acquisition, project administration, resources, supervision, writing – review & editing. **Costa, A.C.:** conceptualization, methodology, supervision, writing – review & editing.

References

- Adler, J.; Parmryd, I., 2010. Quantifying colocalization by correlation: the Pearson correlation coefficient is superior to the Mander's overlap coefficient. *Cytometry Part A*, v. 77 (8), 733-742. <https://doi.org/10.1002/cyto.a.20896>.
- Agência Nacional de Águas (ANA), 2018. Conjuntura dos recursos hídricos no Brasil 2018: informe anual. ANA, Brasília.
- Alvares, C.A.; Stape, J.L.; Sentelhas, P.C.; Gonçalves, J.D.M.; Sparovek, G., 2013. Köppen's climate classification map for Brazil. *Meteorologische Zeitschrift*, v. 22 (6), 711-728. <https://doi.org/10.1127/0941-2948/2013/0507>.
- Alves, J.M.B.; Silva, E.M.D.; Sombra, S.S.; Barbosa, A.C.B.; Santos, A.C.S.D.; Lira, M. A.T., 2017. Eventos extremos diários de chuva no nordeste do Brasil e características atmosféricas. *Revista Brasileira de Meteorologia*, v. 32, 227-233. <https://doi.org/10.1590/0102-77863220012>.
- Back, Á.J.; Cadorin, S.B., 2020. Chuvas extremas e equações intensidade-duração-frequência para o estado do Acre. *Revista Brasileira de Ciências Ambientais*, v. 55 (2), 159-170. <https://doi.org/10.5327/Z2176-947820200597>.
- Berhane, A.; Hadgu, G.; Worku, W.; Abrha, B., 2020. Trends in extreme temperature and rainfall indices in the semi-arid areas of Western Tigray, Ethiopia. *Environmental Systems Research*, v. 9, 1-20. <https://doi.org/10.1186/s40068-020-00165-6>.
- Bhatti, A.S.; Wang, G.; Ullah, W.; Ullah, S.; Fiifi Tawia Hagan, D.; Kwesi Nooni, I.; Lou, D.; Ullah, I., 2020. Trend in extreme precipitation indices based on long term in situ precipitation records over Pakistan. *Water*, v. 12 (3), 797. <https://doi.org/10.3390/w12030797>.
- Bonfim, O.E.T.; Silva, D.F.D.; Kayano, M.T.; Rocha, L.H.D.S., 2020. Análise dos eventos climáticos extremos e de suas causas climáticas para redução de riscos nas bacias hidrográficas Aguapeí e Peixe, São Paulo, Brasil. *Revista Brasileira de Meteorologia*, v. 35 (spe), 755-768. <https://doi.org/10.1590/0102-7786355000004>.
- Brasil, 2022. Ministério das Relações Exteriores. Geografia (Accessed May 12, 2024) at: <https://www.gov.br/mre/pt-br/embaixada-bogota/o-brasil/geografia>.
- Brown, O.L., 1951. The clausius-clapeyron equation. *Journal of Chemical Education*, v. 28 (8), 428. <https://doi.org/10.1021/ed028p428>.

- Caetano, A.L.; da Silva Barbosa, F., 2019. Probabilidade de ocorrência de chuvas extremas para região de Inconfidentes–MG. *Revista Brasileira de Climatologia*, v. 25. <https://doi.org/10.5380/abclima.v25i0.62338>.
- Cardoso, C.D.S.; Quadro, M.F.L.D.; Bonetti, C., 2020. Persistência e abrangência dos eventos extremos de precipitação no Sul do Brasil: Variabilidade espacial e padrões atmosféricos. *Revista Brasileira de Meteorologia*, v. 35, 219–231. <https://doi.org/10.1590/0102-7786352031>.
- Carvalho, A.A.D.; Montenegro, A.A.D.A.; Silva, H.P.D.; Lopes, I.; Morais, J.E.D.; Silva, T.G.D., 2019. Trends of rainfall and temperature in Northeast Brazil. *Revista Brasileira de Engenharia Agrícola e Ambiental*, v. 24 (1), 15–23. <https://doi.org/10.1590/1807-1929/agriambi.v24n1p15-23>.
- Cavalcante, R.B.L.; da Silva Ferreira, D.B.; Pontes, P.R.M.; Tedeschi, R.G.; da Costa, C.P.W.; de Souza, E.B., 2020. Evaluation of extreme rainfall indices from CHIRPS precipitation estimates over the Brazilian Amazonia. *Atmospheric Research*, v. 238, 104879. <https://doi.org/10.1016/j.atmosres.2020.104879>.
- Cavalcanti, I.F., 2016. Tempo e clima no Brasil. Oficina de Textos, [S.l.].
- Chagas, V.B.; Chaffe, P. L.; Blöschl, G., 2022. Process controls on flood seasonality in Brazil. *Geophysical Research Letters*, v. 49 (5), e2021GL096754. <https://doi.org/10.1029/2021GL096754>.
- Clement, C.R.; Higuchi, N., 2006. A floresta amazônica e o futuro do Brasil. *Ciência e Cultura*, v. 58 (3), 44–49. ISSN: 2317-6660.
- Costa, A.C.; Gomes, T.F.; Moreira, R.P.; Cavalcante, T.F.; Mamede, G.L., 2022. Influence of hydroclimatic variability on dengue incidence in a tropical dryland area. *Acta Tropica*, v. 235, 106657. <https://doi.org/10.1016/j.actatropica.2022.106657>.
- Costa, R.L.; de Mello Baptista, G.M.; Gomes, H.B.; dos Santos Silva, F.D.; da Rocha Júnior, R.L.; de Araújo Salvador, M.; Herdies, D.L., 2020. Analysis of climate extremes indices over northeast Brazil from 1961 to 2014. *Weather and Climate Extremes*, v. 28, 100254. <https://doi.org/10.1016/j.wace.2020.100254>.
- da Costa, J.M.F.; Junior, A.D.M.; da Silva Silveira, C.; Júnior, F.D.C.V., 2018. Influência das mudanças climáticas, projetadas pelo IPCC, na aridez do Brasil. *Revista AIDIS de Ingeniería y Ciencias Ambientales. Investigación, Desarrollo y Práctica*, v. 11 (3), 429–442.
- da Silva, D.F.; Lima, M.J.D.S.; Souza Neto, P.F.; Gomes, H.B.; Silva, F.D.D.S.; Almeida, H.R.R.C.; Costa, R.L.; Pereira, M.P.S., 2020. Caracterização de eventos extremos e de suas causas climáticas com base no índice Padronizado de Precipitação Para o Leste do Nordeste. *Revista Brasileira de Geografia Física*, v. 13 (2), 449–464.
- da Silva, P.E.; Silva, C.M.S.; Spyrides, M.H.C.; Andrade, L.D.M.B., 2019. Precipitation and air temperature extremes in the Amazon and northeast Brazil. *International Journal of Climatology*, v. 39 (2), 579–595. <https://doi.org/10.1002/joc.5829>.
- Donat, M.G.; Alexander, L.V.; Yang, H.; Durre, I.; Vose, R.; Dunn, R.J.H.; Willett, K.M.; Aguilar, E.; Brunet, M.; Caesar, J.; Hewitson, B.; Jack, C.; KleinTank, A.M.G.; Kruger, A.C.; Marengo, J.; Peterson, T.C.; Renom, M.; OriaRojas, C.; Rusticucci, M.; Salinger, J.; Elayah, A.S.; Sekele, S.S.; Srivastava, A.K.; Trewin, B.; Villarreal, C.; Vincent, L.A.; Zhai, P.; Zhang, X.; Kitching, S., 2013. Updated analyses of temperature and precipitation extreme indices since the beginning of the twentieth century: The HadEX2 dataset. *Journal of Geophysical Research: Atmospheres*, v. 118 (5), 2098–2118. <https://doi.org/10.1002/jgrd.50150>.
- Donat, M.G.; Lowry, A.L.; Alexander, L.V.; O’Gorman, P.A.; Maher, N., 2016. More extreme precipitation in the world’s dry and wet regions. *Nature Climate Change*, v. 6 (5), 508–513. <https://doi.org/10.1038/nclimate2941>.
- Duarte, T.L.S.; Santos, G.C.; Castelhamo, F.J., 2021. Eventos de chuvas extremas associados aos riscos de inundações e de alagamentos em Aracaju, Sergipe. *GEOSABERES: Revista de Estudos Geoeducacionais*, v. 12, 256–273. <https://doi.org/10.26895/geosaberes.v12i0.1089>.
- Fisch, G.; Marengo, J.A.; Nobre, C.A., 1998. Uma revisão geral sobre o clima da Amazônia. *Acta Amazônica*, v. 28, 101–101. <https://doi.org/10.1590/1809-43921998282126>.
- Flores, B.M.; Montoya, E.; Sakschewski, B.; Nascimento, N.; Staal, A.; Betts, R.A.; Levis, C.; Lapola, D.M.; Esquivel-Muelbert, A.; Jakovac, C.; Nobre, C.A.; Oliveira, R.S.; Borma, L.S.; Nian, D.; Boers, N.; Hecht, S.B.; TerSteege, H.; Arieira, J.; Lucas, I.L.; Berenguer, E.; Marengo, J.A.; Gatti, L.V.; Mattos, C.R.C.; Hirota, M., 2024. Critical transitions in the Amazon forest system. *Nature*, v. 626 (7999), 555–564. <https://doi.org/10.1038/s41586-023-06970-0>.
- Fowler, H.J.; Lenderink, G.; Prein, A.F.; Westra, S.; Allan, R.P.; Ban, N.; Barbero, R.; Berg, P.; Blenkinsop, S.; Do, H.X.; Guerreiro, S.; Haerter, J.O.; Kendon, E.J.; Lewis, E.; Schaer, C.; Sharma, A.; Villarini, G.; Wasko, C.; Zhang, X., 2021. Anthropogenic intensification of short-duration rainfall extremes. *Nature Reviews Earth & Environment*, v. 2 (2), 107–122. <https://doi.org/10.1038/s43017-020-00128-6>.
- Freire, L.L.; Costa, A.C.; Neto, I.E.L., 2023. Effects of rainfall and land use on nutrient responses in rivers in the Brazilian semiarid region. *Environmental Monitoring and Assessment*, v. 195 (6), 652. <https://doi.org/10.1007/s10661-023-11281-y>.
- Gonçalves, S.T.N.; Vasconcelos Júnior, F.D.C.; Silveira, C.D.S.; Cid, D.A.C.; Martins, E.S.P.R.; Costa, J.M.F.D., 2023. Comparative analysis of drought indices in hydrological monitoring in ceará’s semi-arid Basins, Brazil. *Water*, v. 15 (7), 1259. <https://doi.org/10.3390/w15071259>.
- Goudard, G.; Mendonça, F.D.A., 2020. Eventos e episódios pluviais extremos: a configuração de riscos hidrometeorológicos em Curitiba (Paraná-Brasil). *IdeAs. Idées d’Amérique*, (15). <https://doi.org/10.4000/ideas.8082>.
- Griffiths, G.M.; Salinger, M.J.; Leleu, I., 2003. Trends in extreme daily rainfall across the South Pacific and relationship to the South Pacific Convergence Zone. *International Journal of Climatology: A Journal of the Royal Meteorological Society*, v. 23 (8), 847–869. <https://doi.org/10.1002/joc.923>.
- Grimm, A.M.; Zilli, M.T., 2009. Interannual variability and seasonal evolution of summer monsoon rainfall in South America. *Journal of Climate*, v. 22 (9), 2257–2275. <https://doi.org/10.1175/2008JCLI2345.1>.
- Guedes, R.V.S.; do Vale Silva, T.L., 2020. Análise descritiva da precipitação, temperatura, umidade e tendências climáticas no Recife-PE. *Revista Brasileira de Geografia Física*, v. 13 (7), 3234–3253. <https://doi.org/10.26848/rbfg.v13.07.p3234-3253>.
- Haylock, M.R.; Peterson, T.C.; Alves, L.M.; Ambrizzi, T.; Anunciação, Y.M.T.; Baez, J.; Barros, V.R.; Berlato, M.A.; Bidegain, M.; Coronel, G.; Corradi, V.; Garcia, V.J.; Grimm, A.M.; Karoly, D.; Marengo, J.A.; Marino, M.B.; Moncunill, D.F.; Nechet, D.; Quintana, J.; Rebello, E.; Rusticucci, M.; Santos, J.L.; Trebejo, I.; Vincent, L.A., 2006. Trends in total and extreme South American rainfall in 1960–2000 and links with sea surface temperature. *Journal of Climate*, v. 19 (8), 1490–1512. <https://doi.org/10.1175/JCLI3695.1>.
- Hinkle, D.E.; Wiersma, W.; Jurs, S.G., 2003. Applied statistics for the behavioral sciences. v. 663. Houghton Mifflin, Boston.
- Hirsch, R.M.; Slack, J.R.; Smith, R.A., 1982. Techniques of trend analysis for monthly water quality data. *Water Resources Research*, v. 18 (1), 107–121. <https://doi.org/10.1029/WR018i001p0107>.
- Hollins, L.X.; Eisenberg, D.A.; Seager, T.P., 2018. Risk and resilience at the Oroville Dam. *Infrastructures*, v. 3 (4), 49. <https://doi.org/10.3390/infrastructures3040049>.

- Hountondji, Y.C.; De Longueville, F.; Ozer, P., 2011. Trends in extreme rainfall events in Benin (West Africa), 1960-2000. In: 1st International Conference on Energy, Environment and Climate Change. Ho Chi Minh City, Vietnam, 26-27 August.
- Intergovernmental Panel on Climate Change (IPCC), 2023. Climate change 2023: Synthesis report. A report of the Intergovernmental Panel on Climate Change. Contribution of Working Groups I, II and III to the Sixth Assessment Report of the Intergovernmental Panel on Climate Change. IPCC, Geneva, Switzerland.
- Köppen, W., 1936. Das geographische System de Klimate. Handbuch der klimatologie. In: Köppen, W.; Geiger, W. (Eds.), Handbuch der klimatologie. Bd. I. Teil C. Gebrüder Bornträger, Berlin, pp. 1-44.
- Lamb, D.; Verlinde, J., 2011. Physics and chemistry of clouds. Cambridge University Press, Cambridge.
- Liang, X.Z., 2022. Extreme rainfall slows the global economy. *Nature*, v. 601. <https://doi.org/10.1038/d41586-021-03783-x>.
- Lima, K.C.; Satyamurty, P.; Fernández, J.P.R., 2010. Large-scale atmospheric conditions associated with heavy rainfall episodes in Southeast Brazil. *Theoretical and Applied Climatology*, v. 101, 121-135. <https://doi.org/10.1007/s00704-009-0207-9>.
- Loureiro, R.S.D.; Saraiva, J.M.; Saraiva, I.; Senna, R.C.; Fredó, A.S., 2014. Estudo dos eventos extremos de precipitação ocorridos em 2009 no estado do Pará. *Revista Brasileira de Meteorologia*, v. 29, 83-94. <https://doi.org/10.1590/0102-778620130054>.
- Manton, M.J.; Della-Marta, P.M.; Haylock, M.R.; Hennessy, K.J.; Nicholls, N.; Chambers, L.E.; Collins, D.A.; Daw, G.; Finet, A.; Gunawan, D.; Inape, K.; Isobe, H.; Kestin, T.S.; Lefale, P.; Leyu, C.H.; Lwin, T.; Maitrepierre, L.; Ouprasitwong, N.; Page, C.M.; Pahlad, J.; Plummer, N.; Salinger, M.J.; Suppiah, R.; Tran, V.L.; Trewin, B.; Tibig, I.; Yee, D., 2001. Trends in extreme daily rainfall and temperature in Southeast Asia and the South Pacific: 1961-1998. *International Journal of Climatology*, v. 21 (3), 269-284. <https://doi.org/10.1002/joc.610>.
- Marengo, J.A.; Alves, L.M.; Ambrizzi, T.; Young, A.; Barreto, N.J.; Ramos, A.M., 2020. Trends in extreme rainfall and hydrogeometeorological disasters in the Metropolitan Area of São Paulo: a review. *Annals of the New York Academy of Sciences*, v. 1472 (1), 5-20. <https://doi.org/10.1111/nyas.14307>.
- Marengo, J.A.; Cunha, A.P.; Alves, L.M., 2016. A seca de 2012-15 no semiárido do Nordeste do Brasil no contexto histórico. *Revista Climanalise*, v. 3 (1), 49-54.
- Montenegro, S.M.G.L., 2023. Desertificação no Brasil: A exploração não planejada dos recursos naturais e as mudanças climáticas acarretam danos irreversíveis ao meio ambiente. *Ciência e Cultura*, v. 75 (4), 01-07. <http://dx.doi.org/10.5935/2317-6660.20230051>.
- Moreira, R.P.; Costa, A.C.; Gomes, T.F.; de Oliveira Ferreira, G., 2020. Climate and climate-sensitive diseases in semi-arid regions: a systematic review. *International Journal of Public Health*, v. 65, 1749-1761. <https://doi.org/10.1007/s00038-020-01464-6>.
- Nobre, C.A., 2001. Mudanças climáticas globais: possíveis impactos nos ecossistemas do país. *Parcerias Estratégicas*, v. 12, 239-258.
- Paiva, D.F.; Prezoto, H.H.S., 2021. Ciclo das chuvas: uma reflexão sobre o tema. *Biológica-Caderno do Curso de Ciências Biológicas*, v. 3 (1). <https://doi.org/10.5281/zenodo.14014333>.
- Palenzuela, Y.G.; da Silva Texeira, M.; Toledo, D R.; de Fatima Correia, M., 2019. Influência da escala sinótica na evolução de um evento de precipitação extrema na cidade de Pelotas-RS em janeiro de 2009. *Revista Brasileira de Geografia Física*, v. 12 (05), 1770-1783. <https://doi.org/10.26848/rbgf.v12.5.p1770-1783>.
- Pall, P.; Allen, M.R.; Stone, D.A., 2007. Testing the Clausius-Clapeyron constraint on changes in extreme precipitation under CO₂ warming. *Climate Dynamics*, v. 28, 351-363. <https://doi.org/10.1007/s00382-006-0180-2>.
- Peel, M.C.; Finlayson, B.L.; McMahon, T.A., 2007. Updated world map of the Köppen-Geiger climate classification. *Hydrology and Earth System Sciences*, v. 11 (5), 1633-1644. <https://doi.org/10.5194/hess-11-1633-2007>.
- Perez, L.P.; Rodrigues-Filho, S.; Marengo, J.A.; Santos, D.V.; Mikosz, L., 2020. Climate change and disasters: analysis of the Brazilian regional inequality. *Sustainability in Debate*, v. 11 (3), 260-296. <https://doi.org/10.18472/SustDeb.v11n3.2020.33813>.
- Philander, S.G., 1998. Who is El Niño?. *Eos, Transactions American Geophysical Union*, v. 79 (13), 170-170. <https://doi.org/10.1029/98EO00125>.
- Portella, D.A.P.D.C.; Blanco, L.D.S.; Mello Filho, M.E.T.D.; Santos, J.L.A.D., 2022. A importância da Amazônia na dinâmica climática do Centro-Sul Brasileiro. *Revista Ensaios de Geografia*, v. 9 (19).
- Regoto, P.; Dereczynski, C.; Chou, S.C.; Bazzanella, A.C., 2021. Observed changes in air temperature and precipitation extremes over Brazil. *International Journal of Climatology*, v. 41 (11), 5125-5142. <https://doi.org/10.1002/joc.7119>.
- Rocha, V.M., 2021. Um breve comentário a respeito do IPCC AR6. *Entre-Lugar*, v. 12 (24), 396-403. <https://doi.org/10.30612/rel.v12i24.15253>.
- Sanches, R.G.; dos Santos, B.C.; de Figueiredo Neves, G.Z.; Silva, M.S.D.; de Souza, P.H., 2022. Análise da tendência pluviométrica na região central do estado de São Paulo. *Revista Brasileira De Climatologia*, v. 30, 777-797. <https://doi.org/10.55761/abclima.v30i18.15668>.
- Sen, P.K., 1968. Estimates of the regression coefficient based on Kendall's tau. *Journal of the American Statistical Association*, v. 63 (324), 1379-1389. <https://doi.org/10.1080/01621459.1968.10480934>.
- Sena, J.P.O.; Lucena, D.B.; Neto, J.M.M., 2019. Eventos pluviiais intensos e seus impactos em Campina Grande-PB. *Revista de Geociências do Nordeste*, v. 5, 69-77. <https://doi.org/10.21680/2447-3359.2019v5n01D17974>.
- Silva, A.A.; da Franca, R.R., 2021. Identificação e classificação de episódios de chuva extrema no Distrito Federal – Período 1990-2019. *Revista Espaço e Geografia*, v. 24 (2), 134-153. <https://doi.org/10.26512/2236-56562021e40271>.
- Sun, Q.; Zhang, X.; Zwiers, F.; Westra, S.; Alexander, L.V., 2021. A global, continental, and regional analysis of changes in extreme precipitation. *Journal of Climate*, v. 34 (1), 243-258. <https://doi.org/10.1175/JCLI-D-19-0892.1>.
- Tavares, C.D.M.G.; Ferreira, C.D.C.M., 2020. A relação entre a orografia e os eventos extremos de precipitação para o município de Petrópolis-RJ. *Revista Brasileira de Climatologia*, v. 26. <https://doi.org/10.5380/abclima.v26i0.71123>.
- Teixeira, M.D.S.; Prieto, R.B., 2020. Eventos extremos de chuva no Estado do Rio Grande do Sul, Brasil, entre 2004 e 2013. Parte 1: Definição dos eventos e estatísticas. *Revista Brasileira de Meteorologia*, v. 35, 45-52. <https://doi.org/10.1590/0102-7786351027>.
- Teixeira, M.S.; Satyamurty, P., 2007. Dynamical and synoptic characteristics of heavy rainfall episodes in southern Brazil. *Monthly Weather Review*, v. 135 (2), 598-617. <https://doi.org/10.1175/MWR3302.1>.
- Tradowsky, J.S.; Philip, S.Y.; Kreienkamp, F.; Kew, S.F.; Lorenz, P.; Arrighi, J.; Bettmann, T.; Caluwaerts, S.; Chan, S.C.; DeCruz, L.; DeVries, H.; Demuth, N.; Ferrone, A.; Fischer, E.M.; Fowler, H.J.; Goergen, K.; Heinrich, D.; Henrichs, Y.; Kaspar, F.; Lenderink, G.; Nilson, E.; Otto, F.E.L.; Ragone, F.; Seneviratne, S.I.; Singh, R.K.; Skålevåg, A.; Termonia, P.; Thalheimer, L.; VanAalst, M.;

- VandenBergh, J.; VandeVyver, H.; Vannitsem, S.; VanOldenborgh, G.J.; VanSchaeybroeck, B.; Vautard, R.; Vonk, D.; Wanders, N., 2023. Attribution of the heavy rainfall events leading to severe flooding in Western Europe during July 2021. *Climatic Change*, v. 176 (7), 90. <https://doi.org/10.1007/s10584-023-03502-7>.
- Vahedifard, F.; AghaKouchak, A.; Ragno, E.; Shahrokhbabadi, S.; Mallakpour, I., 2017. Lessons from the Oroville dam. *Science*, v. 355 (6330), 1139-1140. <https://doi.org/10.1126/science.aan0171>.
- Wainwright, C.M.; Finney, D.L.; Kilavi, M.; Black, E.; Marsham, J.H., 2021. Extreme rainfall in East Africa, October 2019–January 2020 and context under future climate change. *Weather*, v. 76 (1), 26-31. <https://doi.org/10.1002/wea.3824>.
- Xavier, A.C.; Scanlon, B.R.; King, C.W.; Alves, A.I., 2022. New improved Brazilian daily weather gridded data (1961–2020). *International Journal of Climatology*, v. 42 (16), 8390-8404. <https://doi.org/10.1002/joc.7731>.
- Yaduvanshi, A.; Nkemelang, T.; Bendapudi, R.; New, M., 2021. Os extremos de temperatura e precipitação mudam de acordo com os níveis atuais e futuros de aquecimento global nas zonas climáticas indianas. *Extremos de Tempo e Clima*, v. 31, 100291. <https://doi.org/10.1016/j.wace.2020.100291>.
- Yao, J.; Chen, Y.; Chen, J.; Zhao, Y.; Tuoliewubieke, D.; Li, J.; Yang, L.; Mao, W., 2021. Intensification of extreme precipitation in arid Central Asia. *Journal of Hydrology*, v. 598, 125760. <https://doi.org/10.1016/j.jhydrol.2020.125760>.
- Yeh, S.W.; Kug, J.S.; Dewitte, B.; Kwon, M.H.; Kirtman, B.P.; Jin, F.F., 2009. El Niño in a changing climate. *Nature*, v. 461 (7263), 511-514. <https://doi.org/10.1038/nature08316>.
- Yue, S.; Wang, C., 2004. The Mann-Kendall test modified by effective sample size to detect trend in serially correlated hydrological series. *Water Resources Management*, v. 18 (3), 201-218. <https://doi.org/10.1023/B:WARM.0000043140.61082.60>.
- Zandonadi, L., 2020. Chuvas extremas e o intenso EL Niño de 2015/2016: impactos na rede de coleta e abastecimento de água da cidade de Maringá, Paraná. *Brazilian Geographical Journal: Geosciences and Humanities Research Medium*, v. 11 (1), 38-69. <https://doi.org/10.14393/BGJ-v11n1-a2020-52345>.
- Zhou, H.; Deng, Z.; Xia, Y.; Fu, M., 2016. A new sampling method in particle filter based on Pearson correlation coefficient. *Neurocomputing*, v. 216, 208-215. <https://doi.org/10.1016/j.neucom.2016.07.036>.
- Zhu, W.; Wang, S.; Luo, P.; Zha, X.; Cao, Z.; Lyu, J.; Zhou, M.; He, B.; Nover, D., 2022. A quantitative analysis of the influence of temperature change on the extreme precipitation. *Atmosphere*, v. 13 (4), 612. <https://doi.org/10.3390/atmos13040612>.